Eur. Phys. J. B (2019) 92: 122
https://doi.org/10.1140/epjb/e2019-90715-8

THE EUROPEAN PHYSICAL JOURNAL B

Regular Article

Nonlinear excitations and bound states of electrons, holes and solitons in bilayers of triangular lattices*

Alexander P. Chetverikov[1,2], Werner Ebeling[3], Eckehard Schöll[4,a], and Manuel G. Velarde[1]

[1] Instituto Pluridisciplinar, Universidad Complutense, Paseo Juan XXIII, 1, Madrid 28040, Spain
[2] Department of Physics, Saratov State University, Astrakhanskaya 83, Saratov 410012, Russia
[3] Institute of Physics, Humboldt-University Berlin, Newtonstr. 15, Berlin 12489, Germany
[4] Institute of Theoretical Physics, Technische Universität Berlin, Hardenbergestr. 36, Berlin 10623, Germany

Received 5 December 2018 / Received in final form 18 March 2019
Published online 10 June 2019
© EDP Sciences / Società Italiana di Fisica / Springer-Verlag GmbH Germany, part of Springer Nature, 2019

Abstract. We study the temporal and spatial nonlinear dynamical evolution of a coupled triangular lattice crystal bilayer system where in one layer one excess free electron is injected while an excess positive charge, a hole, is created in the other. The atoms of each of the backbone lattices interact with anharmonic (short range) Morse potentials whereas the charges interact via (long range) Coulomb potentials. Computer simulations are provided of the possibilities offered by varying interlayer separation, strength of the Coulomb force between the charges and the diverse dynamical role played by excited solitons supersonically moving along crystallographic axes in one of the layers. Optimal conditions are identified for the occurrence of electron–hole pairs and for the more significant case of a boson-like electron–hole–soliton coupled compound, a new form of quasiparticle moving along the coupled bilayer system with no need of applying an external electric field.

1 Introduction

The nonlinear dynamics of coupled networks has many diverse applications ranging from big objects like giant electrical power networks to tiny objects like biological cells and neurons [1–7]. While networks are general sets of nodes and links, discrete lattices are special networks where a metric is introduced, and the array of nodes exhibits some translation symmetry (periodicity). Here we focus on the specific case of two nonlinear lattices where in each of them, taken separately, their atoms interact with (short range) Morse forces. Additionally we consider that electrons can be injected in one layer while holes can be created in the other with corresponding (long range) Coulomb interaction between the charges, as well as between the charges and the atoms in the lattice. Such a dynamical system is treated as a mixed classical-quantum system, since the lattice atoms follow Newtonian mechanics, while the charges obey the Schrödinger quantum evolution. We feel that this approach opens the door to novel applications in materials science at the nanolevel, for instance graphene technology.

In general there are two classes of mobile localized excitations in discrete lattices: supersonic soliton-like excitations and subsonic breathers. Lattice solitons were first observed by Toda, who succeeded in finding exact solutions for special one-dimensional lattices [8]. Breathers, which are spatially localized vibrational modes, were first studied in one-dimensional lattices (chains) [9,10]. Here we consider the electron transport assisted by fast soliton-like excitations initiated in a two-dimensional lattice by an initial kick of one soliton along a certain lattice direction. Note that if the kick upon a soliton is strong enough to overcome a potential barrier formed by atoms of adjacent rods (the Peierls–Nabarro barrier), then it is not able to return to its equilibrium state. The localized soliton-like excitation carries an additional quasiparticle along a rod in this case and is called a crowdion [11]. Both the usual soliton-like lattice compression and a crowdion are able to trap an electron and transport it along the lattice. We will call both types *solitons* for simplicity. But note that crowdions, in contrast to usual solitons, shift atoms along their trajectory to the neighbor cells providing a more compact mobile compression of the atomic lattice, i.e., a stronger perturbation, and better conditions for transport of electrons than a usual soliton. That is why in our simulations below we consider soliton-like excitations of crowdion type, by choosing a sufficiently strong initial kick to overcome the potential barrier and shift the kicked atom to the neighbor cell.

* Contribution to the Topical Issue "Non-Linear and Complex Dynamics in Semiconductors and Related Materials", edited by Kathy Lüdge.

[a] e-mail: schoell@physik.tu-berlin.de

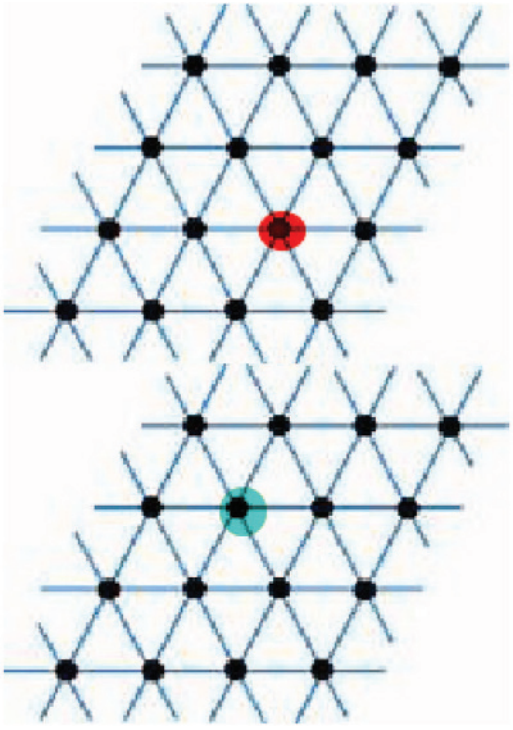


Fig. 1. Bilayer architecture formed of two coupled triangular crystal lattices. We have two networks between two metal gates with an insulating layer in between. An electron can be injected in one layer, here the upper one (identified by a red dot), whereas a hole at the bottom layer can be created (identified by a green dot).

A quasiparticle consisting of a bound soliton and electron will be denoted as *solectron* [12] using the analogy with a polaron [13].

In recent works we discussed already the coupling of electron dynamics to nonlinear excitations in atomic $2d$-lattices. In particular we studied the interaction of acoustic lattice soliton excitations [8] in $2d$-lattices with injected electrons, and found a form of electron surfing [14–16] including effects of degeneracy [17] and transport [18,19]. In particular we discussed also possible applications of controlling electron transport by nonlinear effects [20,21]. The lattice excitations may have different origin such as thermal (heated lattice) or mechanical/electrical shocks generated, e.g., by contacts of the tip of an electron field microscope with the anharmonic crystal lattice layer. In computer simulations we have considered systems of a few hundred atoms on a plane forming triangular [14,15,20] or hexagonal lattices [21].

Here we provide a significant extension of our previous work by considering two coupled triangular lattices separated by a small distance (Fig. 1). A barrier thickness as small as $d \simeq 1$ nm has already been realized with a hexagonal boron nitride dielectric with a dielectric constant $\epsilon \simeq 3$ [22], and interlayer separation distances between 2 nm and 10 nm are already common in experiments with graphene layers. Both of the crystal lattices are doped, the one on top (Fig. 1) with electrons and the bottom layer with holes and, as earlier noted, both are interacting via Coulomb forces and can form a bound quantum state. The lattice units interact via Morse forces. Such an architecture may be of interest for technological applications [23–26,30–32].

The coupling of electrons injected into one layer to holes injected into the other layer has been studied already long ago, including the prediction of possibilities of observing high-temperature electron–hole superfluidity and other interesting effects [23–34]. There is also a large variety of phenomena observed in coupled quantum dots such as mesoscopic bilayers [35–39]. For instance, the recent fabrication of two very close, but electrically insulated, conducting bilayer graphene sheets, one doped with electrons and the other with holes with tunable densities, raises exciting new possibilities [40–42].

In Section 2 we pose the problem and introduce some of the interactions and parameters involved. Section 3 deals with further details on interactions, parameters, and approximations involved in a bilayer architecture. Section 4 provides a discussion of conditions on how solitons assist the formation and transport of electron–hole pairs eventually ending in a boson-like quasiparticle (soliton-e–h). In Section 5 we consider the case of two solitons being excited along different crystallographic axes in such a way to allow their oblique collision. We will show that electron–hole pairing could survive soliton collisions thus offering a way of controlling their transport in the absence of an external electric field. Finally, Section 6 contains a summary of our results, highlighting their significance for novel technological applications.

2 Forces and physical effects

2.1 Atomic interaction

We consider a system consisting of two independently gated layers 1 (upper layer) and 2 (lower layer) separated by a dielectric medium with equal density of electrons in the upper and holes in the lower layer (Fig. 1).

The characteristic length determining the equilibrium distance between lattice atoms is σ which is taken as the length unit. Using the relative distance $r^s = |r_n^s - r_j^s|$ for two atoms in each layer ($s = 1$, upper layer, $s = 2$, lower layer) we set

$$V(r^s) = D\left\{\exp[-2b(r^s - \sigma)] - 2\exp[-b(r^s - \sigma)]\right\}, \quad (1)$$

with constants D, b, σ. By imposing a cutoff of the potential at 1.5σ, we exclude unphysical cumulative interaction effects arising from the influence of lattice units outside the first neighborhood of each atom [14]. Time is measured in units of $1/\omega_M$ which is the inverse frequency of linear oscillations near the minimum of the Morse potential well. By a strong kick at one of the atoms at a boundary we are able to excite running compression waves in the form of supersonic solitons [8]. In Figure 2 we show a such a lattice soliton. For better visualization we have modelled the atoms as small spheres with core electrons represented by a Gaussian distribution centered at each lattice site. In order to follow the evolution of localized excitations we plot the difference $\rho_{\rm ex}$ between the density

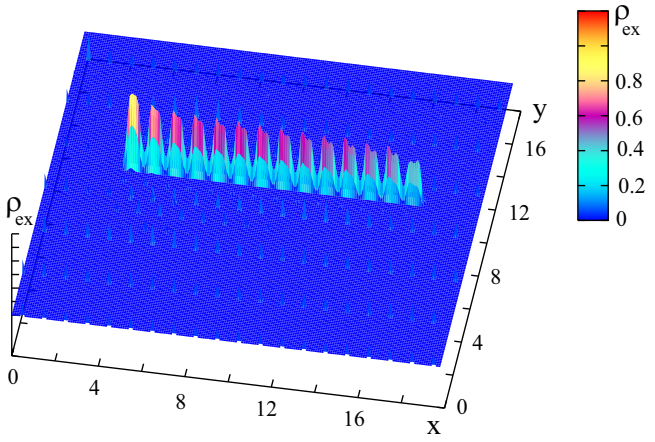


Fig. 2. Single triangular crystal lattice. Soliton-like excitation generated by a kick (a pulse velocity $v_0 = 2$ in units of $\sigma\omega_M$ imposed to one lattice particle near the left border, site 2, row 10) is represented as a bubble-chamber track in a cumulative plot of superposed successive states for the time interval $\Delta t = 3.5$ (measured in units of $1/\omega_M$). The quantity $\rho_{\rm ex}$ denotes the density of atomic core electrons; its zero value corresponds to the initial equilibrium state of the lattice. For the visualization of the atomic positions we consider a Gaussian approximation for such a core electron charge density. (Parameter values: $N = 400$, $b\sigma = 4$, $\lambda = 0.3\sigma$, where λ is the width of the Gaussian.)

of the excited lattice and the equilibrium lattice as a cumulative sequence of snapshots (like in a "bubble chamber representation").

The soliton which is moving along a crystallographic axis (Fig. 2) is excited by a strong pulse of velocity v_0 imposed at $t = 0$ to the 2nd atom in the 10th row with rather high energy $mv_0^2/2$. Such a high-energetic soliton is quite persistent in its motion along the chosen crystallographic axis. Transverse excitations and thermal collisions do not play a significant role in the interval of observation (5 time units measured in units of the inverse linear oscillation frequency defined above).

2.2 Electron–hole interaction

Let us now focus on the electrical interactions between the two coupled lattices. At large separation distances, the two layers are practically uncoupled thus behaving as independent networks [14–16,18,19,21]. When the two layers come closer together, the Coulomb forces between electrons and holes come into play and at small distances e–h pairing can occur. We shall consider the following case: if more than one electron (or hole) exists in a layer, the charge density is low enough to permit neglect of their corresponding Coulomb repulsion. For the electron–hole interaction between an electron in the upper layer (superscript 1) and a hole in the lower one (superscript 2) we assume the Coulomb potential as in [35–38]

$$V_{eh}(x_i^1, y_i^1, x_j^2, y_j^2, d) = -\frac{e^2}{\epsilon[(x_i^1 - x_j^2)^2 + (y_i^1 - y_j^2)^2 + d^2]^{1/2}} = -\frac{e^2}{\epsilon[R^2 + d^2]^{1/2}} \quad (2)$$

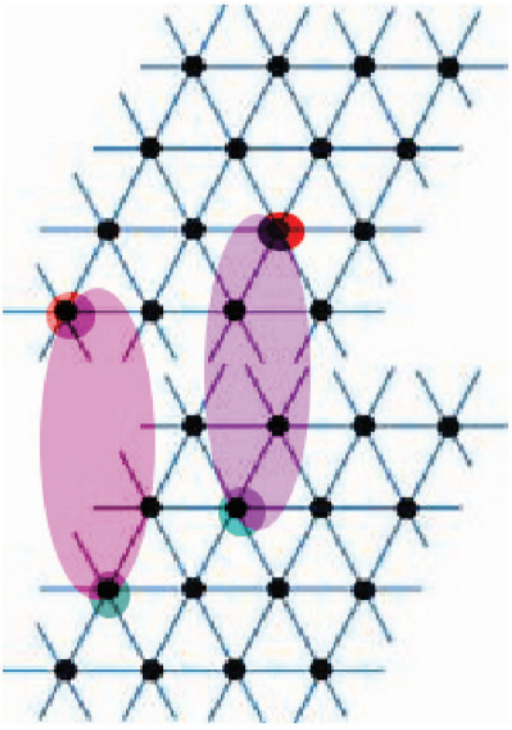


Fig. 3. Bilayer architecture of coupled triangular lattices. The upper layer is doped with electrons and the lower one with holes. At small separation distances the attracting Coulomb forces between electrons and holes eventually lead to e–h-pairing. Note that a dielectric barrier – ruling out tunneling – separates the layers (not drawn here and in the following figures).

where $R^2 = [(x_i^1 - x_j^2)^2 + (y_i^1 - y_j^2)^2]$, $\epsilon \simeq 3$–6 is the effective dielectric constant, $d \simeq 0.1$–$10\,$nm is the distance between the layers, and $x_i^1, y_i^1, x_j^2, y_j^2$ are the coordinates in the upper and lower layer, respectively. This potential is in agreement with the "ansatz" used in [35–38]. In a different context this formula for the Coulomb interaction has been used in earlier work [45]. Efimkin et al. [31] and Conti et al. [33] use Fourier representations for the forces corresponding to a different model. In Figure 3 we discuss the effects due to the Coulomb forces between electrons and holes.

2.3 Electron–soliton interaction

Note, however, that in our computer simulations the electrons and holes are treated quantum mechanically using the tight-binding approximation, which is different from the tools used, e.g., by Conti et al. [33]. As a result the charges "like" to follow the trajectories of soliton-like excitations. Since the soliton is a compression of polarizable atoms we may approximate the interaction between a charge at distance r from a soliton by the polarization potential as often used in plasma physics [14,15]

$$U(r) = -U_e \frac{h^4}{(r^2 + h^2)^2} \qquad U_e \sim \alpha \quad (3)$$

where α is the atomic polarizability and h is the range of the interaction. The constant U_e is in the range 0.05–0.1 eV. The potential U arises from the interaction of an electron with the polarized electron cloud of the atoms. The formula for U is an approximation for the potential between an electron and a polarized hydrogen atom which scales with r^{-4}. Such a potential represents a (moving) potential well in which the electron may be trapped. If the bottom of this well is deep enough and the width is large enough, bound states may be created in the well and the electronic wave function becomes localized. Any displacement of the atoms changes the polarization energy. The charge density will try to follow up these changes thus leading to "solectron" formation [14–16].

Because of symmetry the same may happen with holes leading to hole solectrons. The soliton as it travels disturbs the lattice and emits radiation, a process that occurs in the phonon band. Only after a finite time which is about 5 time units (defined below) in our case the lattice returns to the initially ordered crystalline equilibrium state. Before this relaxation is completed any other soliton trying to cross the trace of a preceding soliton will get stuck.

3 Quantum-mechanical model

3.1 Bound electron–hole pairs

For small enough horizontal distances R of electrons and holes we obtain from equation (2) the Coulomb potential between an electron in layer 1 and a hole in layer 2:

$$V_{eh}(R,d) = -\frac{e^2}{\epsilon d\sqrt{1+(R^2/d^2)}} \simeq \frac{e^2}{\epsilon d}\Big[-1+\frac{R^2}{2d^2}\Big]+\cdots \tag{4}$$

where d is the interlayer spacing. The parabolic approximation corresponds to a two-dimensional harmonic oscillator with frequency ω_{eh} defined by

$$m_{eh}\omega_{eh}^2 = \frac{e^2}{\epsilon d^3}. \tag{5}$$

The minimum of the potential is $-e^2/\epsilon d$, and the quantum-mechanical bound electron–hole states in this potential are given by the Schrödinger equation

$$\Big[-\frac{\hbar^2}{2m_{eh}}\Delta + V_{eh}(R,d)\Big]\psi(R) = E_{n_x,n_y}\psi(R). \tag{6}$$

The energy eigenvalues of the two-dimensional harmonic oscillator are

$$E_{n_x,n_y} = -\frac{e^2}{\epsilon d} + \hbar\omega_{eh}\big[1+n_x+n_y\big] \tag{7}$$

with $n_x, n_y \in \mathbb{N}_0$. The ground state wave function of the e–h pair is given by a Gaussian

$$\psi_{0,0}(R) \sim \exp\Big[-\frac{R^2}{2\alpha_{eh}^2}\Big] \tag{8}$$

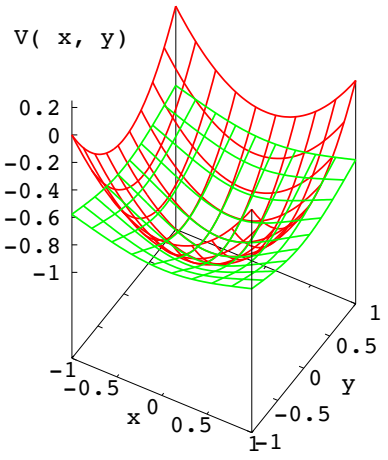


Fig. 4. Potential of the effective force between an electron in layer 1 and a hole in layer 2 (in green). The parabolic approximation (in red) is valid only for small amplitudes.

where

$$\alpha_{eh} = \frac{\hbar}{m_{eh}\omega_{eh}}$$

is the effective horizontal extension of the ground state, and the energy eigenvalue is

$$E_{0,0} = -\frac{e^2}{\epsilon d} + \hbar\omega_{eh}. \tag{9}$$

The condition for the existence of discrete bound states is in this rough approximation

$$\hbar\omega_{eh} < \frac{e^2}{\epsilon d}. \tag{10}$$

The harmonic approximation of the full potential equation (4) for small R is simple but quite limited in validity. In the opposite limit of a strongly anharmonic potential we may use the approximation by Coulomb wave functions, which are characterized by the effective ground state radius α_{eh} of the e–h pair, modified by the effective relative mass m_{eh}/m_e and the dielectric constant ϵ. The effective ground state radius is in first approximation given by the effective Bohr radius

$$a_{eh}^B = a_B\frac{\epsilon}{m_{eh}/m_e} \simeq (0.0529\,\mathrm{nm})\frac{\epsilon}{m_{eh}/m_e} \simeq (1\text{–}5)\,\mathrm{nm}. \tag{11}$$

Here a_B denotes the original Bohr radius for hydrogen. In a variational approach, these wave functions can be used as test functions in the Ritz variational principle to obtain an optimized value a_{eh}^B. We note that Perali et al. [32] estimate for graphene $a_{eh}^B \simeq 8\,\mathrm{nm}$ with a binding energy of 30 meV.

3.2 Conditions for bound electron–hole states

From equation (10) it follows that a bound state exists only if the distance between the layers is sufficiently small, yet not too small, in order to rule out interlayer tunneling. In Figure 5 we show that the bound state pair energy has a minimum at finite values of d, given by

$$d_{\rm opt} \simeq \frac{9}{2} a_{eh}^{B} \simeq (5\text{–}10)\,{\rm nm}. \qquad (12)$$

It is also important that the dielectric constant of the insulating barrier between the electron- and hole-carrying layers is small enough. In any case, the violation of the bound state condition means that the ground state disappears and that instead we have only spatially extended states as we shall see below. For illustration we assume $\epsilon \simeq 3$ and $d \simeq 1\,{\rm nm}$, then we arrive at Bohr radii of a few nm and ground state energies of an order of magnitude around 0.1 eV, or maybe more generally binding energies in the range 10^{-2}–10^{-1} eV. Ground state and structural transitions in mesoscopic electron–hole bilayers have been studied recently in quantum Monte Carlo calculations by Ludwig, Filinov, Bonitz, and Lozovik [38].

A rule of thumb known from plasma physics is that interesting ionization phenomena are to be expected at temperatures around $T \sim 0.1|E_{0,0}/k_B|$ and this estimate in our case leads to temperatures around 100 K (or more generally in the range 10 K–200 K).

3.3 Exciton molecules

Next we discuss the possibility of formation of $(e$–$h)$–$(e$–$h)$ molecules. The Coulomb potential of two electron–hole pairs in a line at distance x is

$$E_0^{(2)}(x) = -2\frac{e^2}{\epsilon d} + \left[2\frac{e^2}{\epsilon x} - 2\frac{e^2}{2\epsilon[x^2+d^2]^{1/2}}\right] \qquad (13)$$

showing that for any positive x-value the formation of double pairs is of no energetic advantage. The only possibility to get negative additional contributions is to introduce materials with quite low dielectric constant or just vacuum between the two layers. We will therefore ignore here the formation of such quasi-"molecules", since quantum effects can only increase the ground state energy. It is the finding of Lozovik and Yudson [23] that excitons in $2d$ repel each other, which ensures the stability of an exciton gas against coalescence into biexcitons, droplets, etc. They also pointed out that this property, which is characteristic for the $2d$ case, makes transitions to a superfluid state possible. Here it is new, in comparison to those studies, that we include the excitation of the solitons, as strong compressions in the lattice as shown in Figure 6.

3.4 Bound electron–hole-soliton states

We will include now a new aspect, the interaction of electron–hole excitations with solitons, as strong compressions in the lattice as shown in Figures 2 and 6. Let us estimate the influence of a soliton upon the ground state energy of an e–h pair. By expanding equation (3) with respect to the horizontal distance r from the polarized atom we obtain

$$U_e(r) = -U_e\frac{h^4}{(r^2+h^2)^2} \simeq -U_e[1 - 2\frac{r^2}{h^2} + \cdots]. \qquad (14)$$

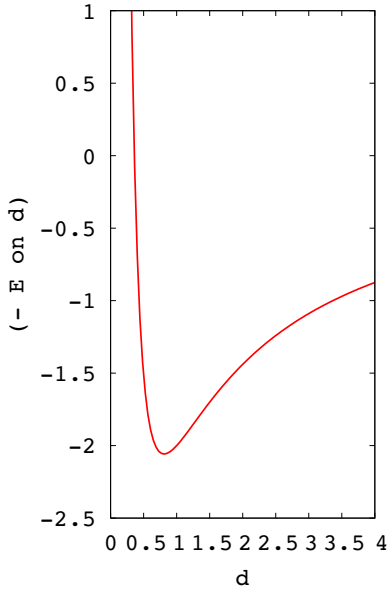


Fig. 5. Ground state energy of an e–h-pair vs. the dimensionless interlayer spacing d.

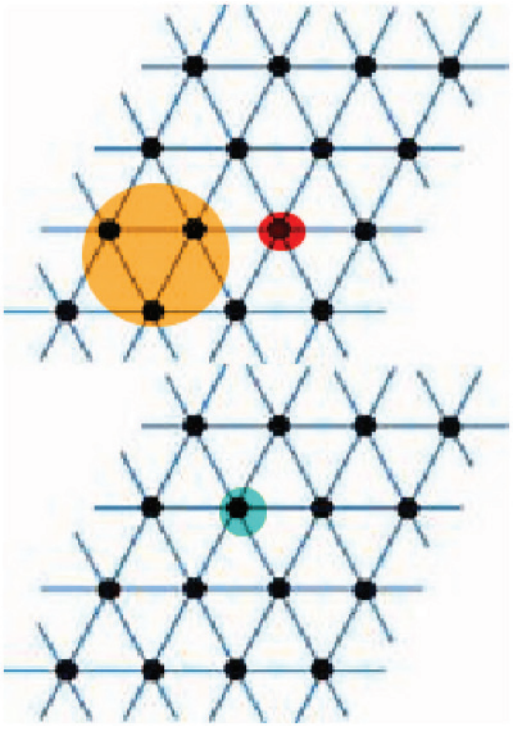


Fig. 6. Bilayer architecture of coupled triangular lattices with one electron (above) and one hole (below) including the excitation of a nearby soliton (here represented by a yellow colored spot).

We assume now that a hole is moving under the simultaneous influence of an electron and a soliton (at the same position) and at a horizontal distance r from that solectron. Then the total potential acting on the hole is

$$V^*_{eh}(R,d) = -\frac{e^2}{\epsilon\sqrt{R^2+d^2}} - U_e\frac{h^4}{(R^2+h^2)^2} \quad (15)$$

$$\simeq -(U_e + \frac{e^2}{\epsilon d}) + \frac{1}{2}a_{eh}R^2 + \cdots \quad (16)$$

with

$$a^*_{eh} = \frac{e^2}{\epsilon d} + 2U_e\frac{1}{h^2}. \quad (17)$$

The effective Schrödinger equation for the states of the electron–hole pair reads

$$\frac{\hbar^2}{2m^*_{eh}}\Delta\psi(R) + [E^{seh}_h - V^*_{eh}(R)]\psi(R) = 0. \quad (18)$$

Here m^*_{eh} is the effective relative mass of the e–h pair in the presence of an excited soliton. Due to the decrease of the lattice distances between atoms in the compression defining the soliton, the effective mass is decreased by the influence of the soliton, $m^*_{eh} < m_{eh}$. Then the ground state of the "dressed" e–h-pair is approximately a Gaussian

$$\psi_{0,0}(R) \sim \exp\Big[-\frac{R^2}{2a^*_{eh}}\Big] \quad (19)$$

where a^*_{eh} is the effective size of the ground state which in harmonic approximation is determined by the oscillator frequency of the electron–hole oscillations around the potential minimum

$$(\omega^*_{eh})^2 = \frac{e^2}{m^*_{eh}\epsilon d^3} + 4\frac{U_e}{m^*_{eh}h^2} \quad (20)$$

and the ground state of the two-dimensional e–h pair dressed by the presence of a soliton is given by

$$E^*_{eh} = -(U_e + \frac{e^2}{\epsilon d}) + \hbar\omega^*_{eh}. \quad (21)$$

In harmonic approximation the ground state levels of the "dressed" pair are modified by two effects:

- deepening of the well by the compression along the lattice
- decrease of the mass of the pair since the compressions enhance transitions.

The condition for the existence of bound states is that at least the ground state is $E^*_{eh} < 0$, and this is a condition on the parameters which reads explicitly

$$-(U_e + \frac{e^2}{\epsilon d}) + \hbar\omega^*_{eh} < 0. \quad (22)$$

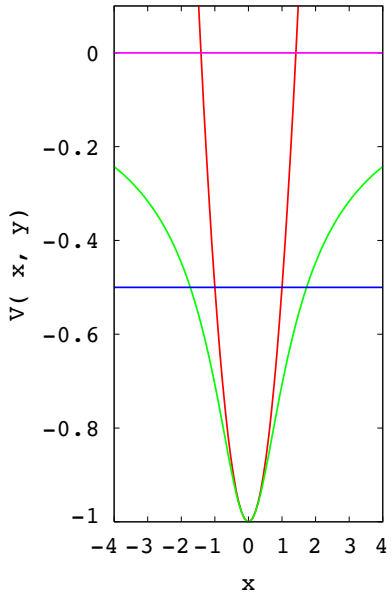


Fig. 7. Illustration of the formation of a localized (bound) e–h state in a potential well created by an electron supported by a soliton. The quantum state extends only over 2–10 lattice sites and the size is strongly increasing for higher levels. Green and red refer to full theory and linearized form, respectively.

If this condition is violated, the ground state disappears and instead we have only spatially extended states. In order to estimate the influence of solitons, or compressions in other similar cases, we have to compare with the condition without compressions

$$-\frac{e^2}{\epsilon d} + \hbar\omega^*_{eh} < 0. \quad (23)$$

Evidently the inequality (22) is easier to fulfil than the inequality (23). In other words, the existence of other forms of nonlinear lattice compressions favors the formation of pairs, as demonstrated in Figure 7. So far we have assumed that solitons and electrons have a definite position near to each other. In a concrete physical situation the density of solitons, and the probability that electron and soliton meet, have to be considered. The essential point, however, remains true: the existence of solitons or some other energy-rich excitations of the lattice contributes to the localization of the electrons and thus it may favor the formation of electron–hole pairs.

4 Soliton-assisted formation and transport of electron–hole pairs

4.1 Quantum dynamics of electron–hole pairs without soliton

Here we consider the case of the boson-like electron–hole-soliton quasiparticle. Figure 8 illustrates the formation of electron–hole pairs by mere application of quantum mechanics in the presence of lattice deformations but

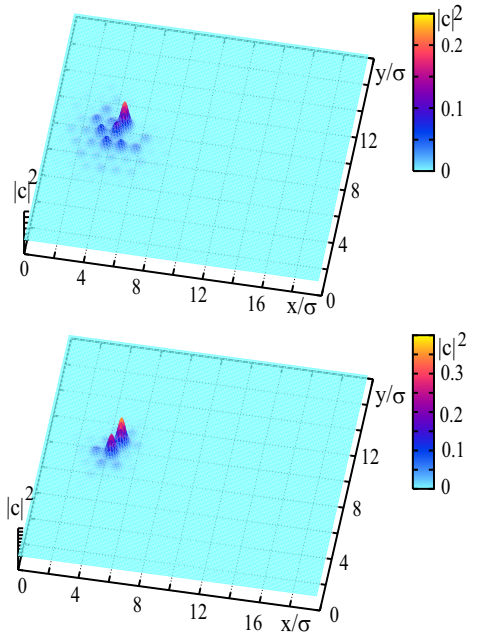


Fig. 8. Bilayer architecture of coupled triangular lattices ($N = 400$) in the absence of soliton excitations. The charge distribution of an electron–hole pair is represented by the probability densities of an electron $|c_n^1|^2$ in the top layer (upper panel) and a hole $|c_n^2|^2$ in the bottom layer (lower panel). Both are to be considered as localized (yet distributed over 5–20 lattice sites) due to quantum mechanics corresponding to high coupling parameter ($\tau_{eh} = 300$; other parameter values: $N = 400, b\sigma = 4, V = 1, \alpha = 1.5, \tau = 10, d = 5\sigma, r_{cut} = 5$).

no solitons. The Hamiltonian of each separate triangular lattice (denoted by 1 and 2) is

$$H_a = H_a^1 + H_a^2$$

$$H_a^s = \frac{m}{2}\sum_n (v_n^s)^2 + \frac{1}{2}\sum_{n,j} V(r_n^s,\, r_j^s). \qquad (24)$$

The subscripts a denote the atoms, all with equal mass m, at the lattice sites, and the summations over n, j run from 1 to N in the upper and lower lattice (superscript s), respectively. The electronic Hamiltonian for the bilayer architecture of coupled lattices consists of three parts for electrons (e), holes (h), and Coulomb interaction (V_{eh}):

$$H_{eh}^s = H_e + H_h + V_{eh}. \qquad (25)$$

In order to study the evolution of the quantum states of the excess electrons and holes interacting with the atomic lattice sites we use the tight-binding approximation thus restricting our consideration to hopping processes between the lattice sites. The electrons are localized at lattice sites, and $|c_n|^2$ is the probability of finding an electron at lattice site n (see, e.g. [14,15]). Further, for simplicity we consider only one electron in the upper layer ($s = 1$), and one hole in the lower layer ($s = 2$). In second quantization formalism the electron part is

$$H_e = \sum_n E_n^1 c_n^{1+} c_n^1 + \sum_{n,n'} t_{n,n'}(\mathbf{r}_{n'}^1 - \mathbf{r}_n^1) c_{n'}^{1+} c_n^1, \qquad (26)$$

where E_n^1 is the single-electron energy, c_n^{1+}, c_n^1 are electron creation and annihilation operators, respectively, and $t_{n,n'}$ is the transition matrix. The analogous contribution of the holes is

$$H_h = \sum_n E_n^2 c_n^{2+} c_n^2 + \sum_{n,n'} t_{n,n'}(\mathbf{r}_{n'}^2 - \mathbf{r}_n^2) c_{n'}^{2+} c_n^2. \qquad (27)$$

Here we assume only one quantum state of electrons/holes per lattice site and transitions between $\mathbf{r}_n$ and $\mathbf{r}'_n$.

4.2 Electron–hole pairs dressed by solitons

To study the nonlinear excitations of the lattice and electron transport in a lattice in the simplest approximation it is sufficient to know the coordinates of the lattice point of the particles at each time and the interaction of lattice deformations with the electrons/holes. The coordinates of the particles are obtained by solving Newton's equations of motion for each lattice point under the influence of all forces, including very weak friction and random forces if one wishes to extend the description to a stochastic Langevin model. For convenience, we use complex coordinates $Z^s = x^s + iy^s$, where x^s and y^s are Cartesian coordinates. Further $Z_{nk}^s = Z_n^s - Z_k^s$ and $z_{nk} = (Z_n - Z_k)/|Z_n - Z_k|$ is the unit vector defining the direction of the interaction force F_{nk}, corresponding to the Morse potential, between the nth and the kth units in the lattice.

To obtain dimensionless variables we rescale the spatial coordinates by σ as length unit. Time is normalized to the inverse frequency of linear oscillations near the minimum of the Morse potential well, ω_M^{-1}, whereas energy is scaled with $2D$. In view of the above, only those lattice units with coordinates Z_k, satisfying the condition $|Z_n - Z_k| < 1.5$, are taken into account. The initial condition is defined by the distribution corresponding to the minimum of potential energy for an equilibrium state of a *triangular* lattice $20\sigma \times 20\sigma$. As already noted, for visualization and tracking the atomic electron densities the lattice atoms are taken as little spheres with "core" electrons represented by a corresponding Gaussian distribution centered at each lattice site:

$$\rho_n(Z^s, t) \sim \sum_{|Z^s - Z_n^s(t)| < 1.5} \exp\left[-\frac{|Z^s - Z_n^s(t)|^2}{2\lambda^2}\right]. \qquad (28)$$

Using the trajectories of particles $Z_n^s(t)$ in layer s and their velocities we can calculate the lattice atom distribution $\rho(Z^s, t)$. In the $2d$ triangular Morse lattice v_{sound} is slightly above 1 in our units. These features point to soliton-like behavior. Indeed, the solitons move for a few picoseconds with almost unaltered profile, and this robustness is the reason why we can identify them with the proposed visualization method. Losses due to scattering

and radiation of linear waves are quite low, due to the almost integrable character of the problem. Note that the $2d$ solitons observed here are similar to the so-called lump solutions of the Kadomtsev–Petviashvili equation [8,14,15].

4.3 Electron–hole transport

Let us now focus on the role played by one or several non-interacting excess electrons injected into the atomic lattice. Following Davydov, we assume that a soliton is connected with a deformation density of the lattice along its path. The transition matrix elements $t_{n,n'}$ depend on the atomic distances, $t_{n,n'} = t(\mathbf{r}_{n'} - \mathbf{r}_n)$. Following Slater

$$t_{n,n'} = V_0 \exp[-\alpha_h |\mathbf{r}_n - \mathbf{r}_{n'}|]. \tag{29}$$

The range parameter α_h can be related to the tunneling probability that decreases exponentially with distance.

The contribution V_{eh} describes the electrical coupling between the electron in the upper lattice 1 and the hole in the lower lattice 2

$$V_{eh}(1,2) = V_{eh0} \sum_{n>m} V_{n,m} |c_n^1|^2 |c_m^2|^2 \tag{30}$$

with

$$V_{eh0} = -\frac{e^2}{\epsilon}; \qquad V_{n,m} = \frac{1}{[|Z_n^1 - Z_m^2|^2 + d^2]^{1/2}}. \tag{31}$$

For the charge dynamics N Schrödinger equations in tight-binding approximation for the complex amplitudes c_n^s are given in dimensionless units for the upper layer

$$i\frac{dc_n^1}{dt} = \epsilon_0 c_n^1 - \tau_{eh} \sum_m V_{nm} |c_m^2|^2 c_n^1 - \tau \exp(\alpha b\sigma) \sum_{k,|Z_n^1 - Z_k^1| < r_{cut}} \left[c_k^1 \exp(-\alpha |Z_n^1 - Z_k^1|) \right] \tag{32}$$

and the lower layer

$$i\frac{dc_n^2}{dt} = \epsilon_0 c_n^2 - \tau_{eh} \sum_m V_{m,n} |c_m^1|^2 c_n^2 - \tau \exp[\alpha b\sigma] \sum_{k,|Z_n^2 - Z_k^2| < r_{cut}} c_m^2 \exp(-\alpha |Z_n^2 - Z_m^2|). \tag{33}$$

Here we use $\tau = V_0/\hbar\omega_0$, $\alpha = \alpha_h \sigma$. We do not assume any regular order of the atoms, except at $t = 0$, where the triangular lattice configuration is assumed at equilibrium. The constant normalized energy $\epsilon_0 = E_n^s/(2D)$ of electrons at lattice site n is irrelevant for the dynamics and may be put equal to zero. As already indicated, the sum over $m \neq n$ in the coupling term is extended over pairs with distance smaller than 1.5σ. Then the complete set of evolution equations is given by equations (32) and (33). Newton's equations for atoms in layers 1 and 2 read:

$$\frac{d^2 Z_n^{1,2}}{dt^2} = \sum_{|Z_n^{1,2} - Z_m^{1,2}| < 1.5} \Big[\exp(b\sigma - |Z_n^{1,2} - Z_m^{1,2}|) \times (1 - \exp(b\sigma - |Z_n^{1,2} - Z_m^{1,2}|) + 2\alpha V \exp(\alpha(b\sigma - |Z_n^{1,2} - Z_m^{1,2}|)) \Big] \times \mathrm{Re}(c_n c_m *) \frac{Z_n^{1,2} - Z_m^{1,2}}{|Z_n^{1,2} - Z_m^{1,2}|},$$

where $V = V_0/(2D)$. We assume that in our case the feedback from the electron dynamics to the lattice dynamics, i.e., the polaron effect is weak and may be neglected in first approximation. That means that we consider the mechanical excitations strong enough to dominate the time and space evolution of the bilayer architecture of coupled lattices.

Figure 8 illustrates the formation of an electon–hole pair via Coulomb interaction when no solitons are excited. Pairing is possible when the Coulomb force is strong enough, here $\tau_{eh} = 300$. When the Coulomb force is weaker, e.g., $\tau_{eh} = 150$, we find that no pairs are formed. Figure 9 shows that electrons and holes tend to delocalize as a consequence of their independent quantum mechanical evolution. Figure 10 shows the case of a further weakened Coulomb force. Even though there are

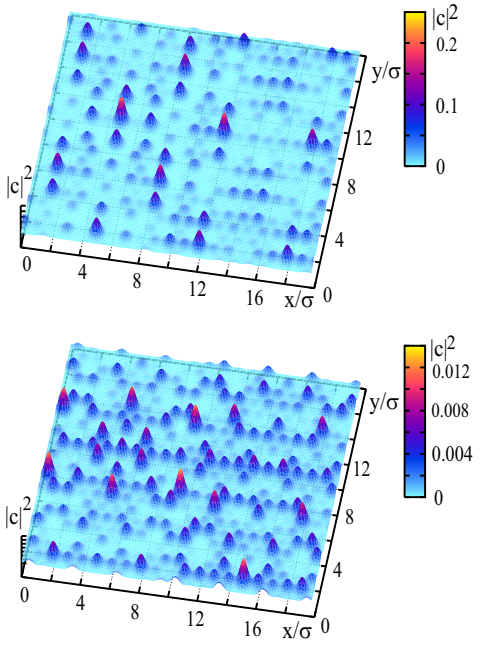


Fig. 9. Bilayer architecture of coupled triangular lattices ($N = 400$) in the absence of soliton excitation though both lattices are (polaronically) perturbed. For not too strong coupling $\tau_{eh} = 150$, the probability distribution to find an electron in the upper layer (top panel) and to find a hole in the lower layer (bottom panel) are only loosely correlated, and we see stochastically independent, almost uniform distributions in both lattices. Snapshots at a certain time are shown. Parameter values are the same as in Figure 8.

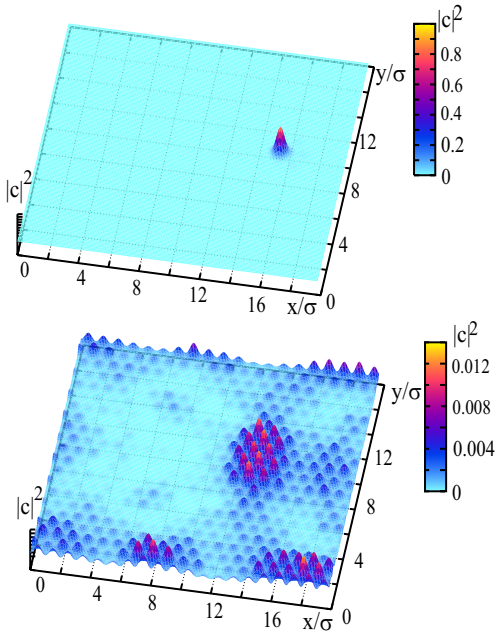


Fig. 10. Bilayer architecture of coupled triangular lattices ($N = 400$) in the presence of soliton excitations. The pair formation tends to be favored by the presence of a nearby soliton since the soliton deepens the potential well and enhances transitions. However, in the top layer the strong soliton carries the electron to the right boundary, while after a short time the hole is lost since the e–h coupling is too weak ($\tau_{eh} = 50$) and therefore the hole probability density disperses. Parameter values characterizing the soliton are the same as in Figure 2, and parameter values characterizing electron-soliton interaction in a layer are the same as in Figure 8.

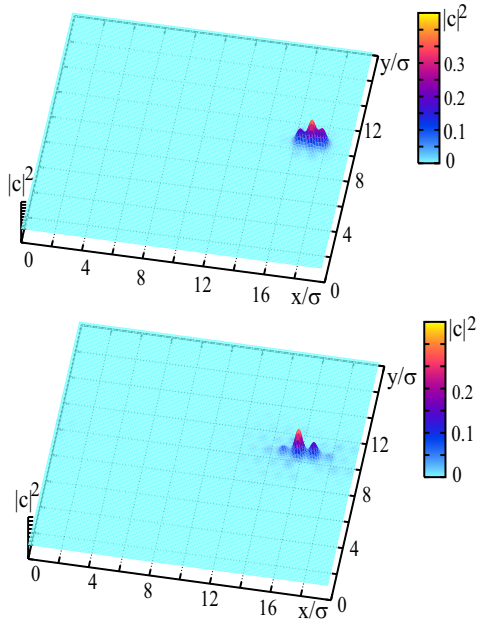


Fig. 11. Bilayer architecture of coupled triangular lattices ($N = 400$) in the presence of a soliton excitation. Shown is the case of trapping an electron–hole pair by a strong soliton in the upper layer which started at the left boundary of the lattice when $\tau_{eh} = 300$ as in Figure 8. The unperturbed second lattice (lower layer) has no soliton but nevertheless the hole follows in parallel the path taken by the electron and the soliton. It clearly appears that a soliton may be used for controlling the path of the e–h pair. The trajectory of the soliton not shown here is rectilinear from left to right as shown in Figures 2 and 6. The parameter values are the same as in Figures 2 and 8 except τ_{eh}.

soliton excitations in the upper (electron) lattice they do not appear capable of sustaining an initially soliton-assisted e–h compound. Finally in Figure 11 a situation similar to Figure 8, but with strong soliton excitation in the electron lattice (upper layer), is shown. It is strong enough to bind the electron, and with a sufficiently strong Coulomb attraction ($\tau_{eh} = 300$) a boson-like compound soliton electron–hole is formed, which travels for a long time along the lattice crystal.

5 Control of e–h pair dynamics by collisions betweens solitons

Let us now consider the case where two solitons collide at an angle and yet the electron–hole pair survives. Further, electron–hole pair transport is enabled from a given entry gate to a chosen exit gate with no need of applying an external electric field.

In the preceeding section we have considered the role played by a single soliton excitation in assisting the formation and transport of an electron–hole pair. This is a consequence of three-body dynamics. Here we will discuss what happens if a second soliton collides under an angle with the first soliton, in particular, how this affects the electron–hole pair and its transport.

Earlier we investigated the effects due to crossing solitons [21] when a single excess electron in a single layer is injected. We showed that crossing solitons may be of interest as a means of controlling electron transport, e.g., by transferring the charge from an entry gate to a chosen exit gate, as in a transistor [21].

Figures 12 and 13 show the results of the interaction of an electron–hole pair with two nearby solitons as a 4-body problem. In spite of the complexity of this interaction process it may be used for the control of the motion of e–h-pairs. This is clearly seen in Figure 14 which shows the electron and hole probability distributions for the crossing soliton dynamics in Figure 13.

What happens in Figure 12 is that the electron and the hole bound to a soliton that started their common path at the left boundary, after colliding with a second soliton excited at the bottom boundary with a 60° angle in its path, leave the initial soliton and continue their path bound to the second soliton along the direction at an angle of 60°. A similar situation occurs with a 120° collision angle as shown in Figures 13 and 14. This clearly demonstrates how the path of an e–h-pair can be guided by appropriate soliton excitation in a kind of metaphoric "promiscuity" effect. Indeed, the electron–hole pair transport is first assisted by one soliton and subsequently the e–h pair moves with the other crossing soliton.

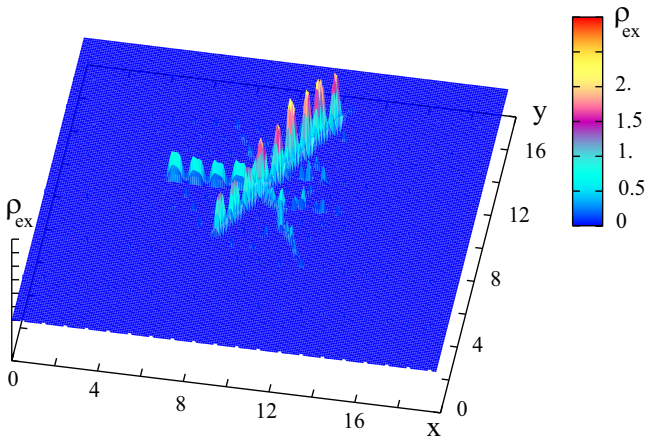


Fig. 12. Bilayer architecture of two coupled crystal lattices ($N = 400$; only the upper layer is shown). The simulation shows the result obtained after the soliton carrying the e–h pair collides with a second soliton like the first one but arriving at an angle of 60°. After the collision the e–h pair is transported by the second soliton. Parameter values are the same as in Figure 11.

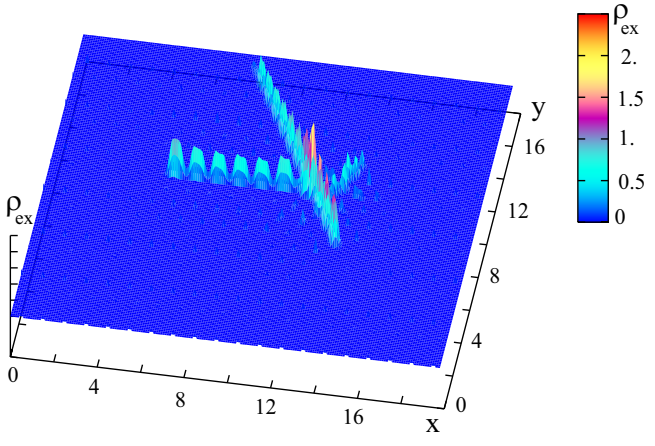


Fig. 13. Bilayer architecture of two coupled crystal lattices ($N = 400$; only the upper layer is shown). The simulation shows the result obtained after the soliton carrying the e–h pair collides with a second soliton like the first one but arriving at an angle of 120°. After the collision the e–h pair is transported by the second soliton. Parameter values are the same as in Figure 11.

Similar effects are to be expected for alternative lattice compressions such as mobile breathers, since in fact we did not use any specific mathematical property of solitons except that they are robust local lattice compressions which induce polarization effects in the crystal lattices.

6 Conclusion

In earlier works it was established that soliton-assisted electron surfing is possible in single layers of a crystal lattice of various topologies [2–4,6–8]. In the present work

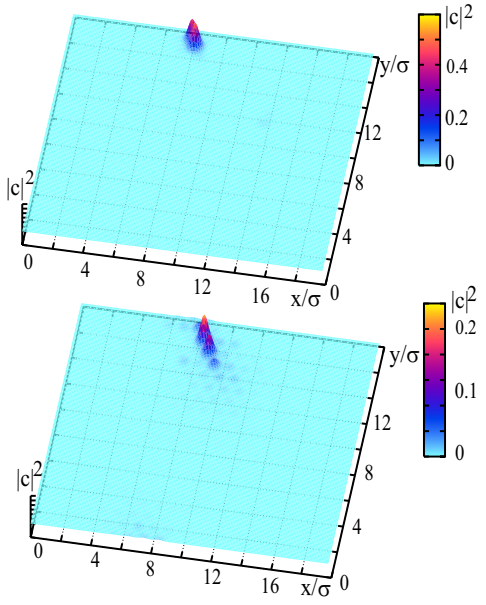


Fig. 14. Bilayer architecture of two coupled triangular lattices ($N = 400$) corresponding to Figure 13. Here the electron and hole probability densities are shown: electrons in the upper layer (top panel) and holes in the lower layer (bottom panel) after the collision where the e–h pair is taken over from the first soliton and subsequently transported by the second soliton. Parameter values are the same as in Figure 13.

we have extended the study to the case of two coupled layers. First we have shown that if in one layer an excess electron is injected and in the other layer a hole is created, electron–hole pair formation depends indeed on the strength of the corresponding Coulomb attraction and the interlayer spacing, provided the spacing is above a minimum value to rule out tunneling. Then we have studied the influence of solitons excited in one of the layers, here in the upper (electron) layer. It appears that such lattice disturbances, with the resulting polarization, significantly increase the depth of the attractive potential between electron and hole. Further, we have illustrated various possibilities of control offered by varying the strength of the Coulomb attraction, the role of the interlayer separation and the role of the lattice soliton. Then we have provided computational evidence of how the soliton/crowdion-assisted surfing is possible for electron–hole pairs with formation of a soliton-electron–hole Boson like compound (consequence of three-body dynamics). Finally, we have shown that when more than one soliton is excited in a lattice, possible crossing processes of the solitons can permit, following four-body dynamics, the nano-mechanical control and transport of electron–hole pairs, if one wishes to bring such a pair from a given entry gate to a chosen exit gate. We propose that the results reported offer prospects for novel technologies in nano-electronics. Moreover, further features of the formation of bosonic electron–hole atoms including mass action laws and possible Bose–Einstein condensation of e–h-atoms [33,34] should be explored.

This work was supported by the Deutsche Forschungsgemeinschaft (DFG, German Research Foundation) – Projektnummer – 163436311 – SFB 910 *Control of self-organizing nonlinear systems: Theoretical methods and concepts of application* (SFB 910).

Author contribution statement

APC did the numerical simulations. All authors designed the study and contributed to the preparation of the manuscript. All authors have read and approved the final manuscript.

References

1. S.H. Strogatz, Nature **410**, 268 (2001)
2. R. Albert, A.L. Barabási, Rev. Mod. Phys. **74**, 47 (2002)
3. M.E.J. Newman, SIAM Rev. **45**, 167 (2003)
4. S. Boccaletti, G. Bianconi, R. Criado, C.I. del Genio, J. Gómez-Gardeñes, M. Romance, I.S. Nadal, Z. Wang, M. Zanin, Phys. Rep. **544**, 1 (2014)
5. M. Kivelä, A. Arenas, M. Barthélemy, J.P. Gleeson, Y. Moreno, M.A. Porter, J. Complex Netw. **2**, 203 (2014)
6. M. De Domenico, V. Nicosia, A. Arenas, V. Latora, Nat. Commun. **6**, 6864 (2015)
7. S. Boccaletti, A.N. Pisarchik, C.I. del Genio, A. Amann, *Synchronization: From Coupled Systems to Complex Networks* (Cambridge University Press, Cambridge, 2018)
8. M. Toda, *Theory of Nonlinear Lattices*, 2nd edn. (Springer-Verlag, New York, 1989)
9. A.J. Sievers, S. Takeno, Phys. Rev. Lett. **61**, 970 (1988)
10. R.S. MacKay, S. Aubry, Nonlinearity **7**, 1623 (1994)
11. H.R. Paneth, Phys. Rev. **80**, 708 (1950)
12. M.G. Velarde, W. Ebeling, A.P. Chetverikov, Int. J. Bifurc. Chaos **15**, 245 (2005)
13. L.D. Landau, Phys. Z. Sowjetunion **3**, 644 (1933)
14. A.P. Chetverikov, W. Ebeling, M.G. Velarde, Eur. Phys. J. B **70**, 217 (2009)
15. A.P. Chetverikov, W. Ebeling, M.G. Velarde, Eur. Phys. J. B **80**, 137 (2011)
16. A.P. Chetverikov, W. Ebeling, G. Röpke, M.G. Velarde, Contrib. Plasma Phys. **51**, 814 (2011)
17. A.P. Chetverikov, W. Ebeling, M.G. Velarde, Toward a theory of degenerated solectrons in doped lattices, in *Without bounds a scientific canvas of nonlinearity and complex dynamics*, edited by R.G. Rubio et al. (Springer, Berlin 2013)
18. A.P. Chetverikov, W. Ebeling, M.G. Velarde, Eur. Phys. J. B **85**, 291 (2012)
19. A.P. Chetverikov, W. Ebeling, G. Röpke, M.G. Velarde, Eur. Phys. J. B **87**, 153 (2014)
20. A.P. Chetverikov, W. Ebeling, M.G. Velarde, Eur. Phys. J. B **89**, 196 (2016)
21. A.P. Chetverikov, W. Ebeling, E. Schöll, M.G. Velarde, Int. J. Dyn. Control **6**, 1376 (2018)
22. R.V. Gorbachev, A.K. Geim, M.I. Katsnelson, K.S. Novoselov, T. Tudorovskiy, Nat. Phys. **8**, 896 (2012)
23. Y.E. Lozovik, V.I. Yudson, JETP Lett. **22**, 274 (1975)
24. Y.E. Lozovik, V.I. Yudson, Sov. Phys. JETP **44**, 389 (1976)
25. S. Shevchenko, Sov. J. Low Temp. Phys. **2**, 251 (1976)
26. Y.E. Lozovik, O.L. Berman, Pis'ma Zh. Eksp. Teor. Fiz. **64**, 526 (1996)
27. Y.E. Lozovik, O.L. Berman, JETP Lett. **64**, 573 (1996)
28. Y.E. Lozovik, O.L. Berman, Zh. Eksp. Teor. Fiz. **111**, 1879 (1997)
29. Y.E. Lozovik, O.L. Berman, JETP **84**, 1027 (1997)
30. P. Eisenstein, A.H. MacDonald, Nature **432**, 691 (2004)
31. D.K. Efimkin, V.A. Kulbachinskii, Y.E. Lozovik, JETP Lett. **93**, 219 (2011)
32. A. Perali, D. Neilson, A.R. Hamilton, Phys. Rev. Lett. **110**, 146803 (2013)
33. S. Conti, A. Perali, F.M. Peeters, D. Neilson, arXiv.1706.07672 (2017)
34. A. Perali, S. Conti, F.M. Peeters, N. Neilson, in *International Conference Strongly Coupled Coulomb Systems, Kiel, 30 July–4 August 2017*
35. A. Filinov, M. Bonitz, Y.E. Lozovik, Phys. Rev. Lett. **86**, 3851 (2001)
36. A. Filinov, M. Bonitz, Y.E. Lozovik, Phys. Stat. Sol. (b) **221**, 231 (2000)
37. M. Bonitz, V. Golubnychij, A.V. Filinov, Y.E. Lozovik, Microelectron. Eng. **63**, 141 (2002)
38. P. Ludwig, A.V. Filinov, M. Bonitz, Y.E. Lozovik, Contrib. Plasma Phys. **43**, 285 (2003)
39. J. Schleede, A. Filinov, M. Bonitz, H. Fehske, Contr. Plasma Phys. **52**, 10 (2012)
40. A.K. Geim, I.V. Grigorieva, Nature **499**, 419 (2013)
41. K. Lee, J. Xue, D.C. Dillen, K. Watanabe, T. Taniguchi, E. Tutuc, Phys. Rev. Lett. **117**, 046803 (2016)
42. J. Li, T. Taguchi, K. Watanabe, J. Hone, A. Levchenko, C. Dean, Phys. Rev. Lett. **117**, 046802 (2016)
43. M.G. Velarde, A.P. Chetverikov, W. Ebeling, S.V. Dmitriev, V.D. Lakhno, Eur. Phys. J. B **89**, 233 (2016)
44. S.V. Dmitriev, E.A. Korznikova, Y.A. Baimova, M.G. Velarde, Phys. Uspekhi **59**, 446 (2016)
45. A. Chetverikov, W. Ebeling, G. Röpke, M.G. Velarde, Contrib. Plasma Phys. **47**, 465 (2007)
46. W. Ebeling, V.E. Fortov, V. Filinov, *Quantum Statistics of Dense Gases and Nonideal Plasmas* (Springer, Berlin, Heidelberg, 2017)
47. A.V. Savin, Z.S. Kivshar, R. Hu, Phys. Rev. B **82**, 195422 (2010)